Damage evolution on Sm and O sublattices in Au-implanted samarium titanate pyrochlore

Y. Zhang,[a] W. J. Weber, V. Shutthanandan, R. Devanathan, and S. Thevuthasan
Pacific Northwest National Laboratory, Richland, Washington

G. Balakrishnan and D. M. Paul
Department of Physics, University of Warwick, Coventry, United Kingdom

(Received 16 July 2003; accepted 8 December 2003)

Damage evolution on the Sm and O sublattices in $Sm_2Ti_2O_7$ single crystals irradiated with 1 MeV Au^{2+} ions at 170, 300, and 700 K was studied by Rutherford backscattering spectroscopy and $^{16}O(d,p)^{17}O$ nuclear reaction analysis along the ⟨001⟩ direction. The damage accumulation behavior at each irradiation temperature indicates that the relative disorder on the O sublattice is higher than that on the Sm sublattice, and the relative disorder, determined by ion channeling, on each sublattice follows a nonlinear dependence on dose that is well described by a disorder accumulation model. While there is little difference in damage accumulation behavior on the Sm sublattice at 170 and 300 K irradiation, the rate of damage accumulation decreases dramatically at 700 K due to dynamic recovery processes. The critical dose for amorphization at 170 and 300 K is 0.14 displacements per atom (dpa), and a higher dose of 0.22 dpa is observed under irradiation at 700 K. During thermal annealing in an ^{18}O environment, a significant increase in the ^{18}O exchange was observed between 800 and 900 K, which is just below the previously determined critical temperature, 950 K, for amorphization in $Sm_2Ti_2O_7$, suggesting that the mobility of O vacancies may be important in defining the critical temperature. © *2004 American Institute of Physics.*
[DOI: 10.1063/1.1644891]

I. INTRODUCTION

Pyrochlore materials, due to the remarkable elemental versatility in the $A_2B_2O_7$ crystal structure, are considered for a wide range of applications, such as fuel cells,[1,2] catalysts,[3,4] and the immobilization of actinide-rich nuclear waste[5–7] or excess plutonium.[8,9] Considerable self-radiation damage from alpha-decay in actinide-bearing phases can result in amorphization, macroscopic swelling, and order-of magnitude increases in dissolution rates,[10–13] and these changes in structure and chemical durability affect long-term performance of the actinide waste forms.[9–15] Studies of actinide-doped[11,12,16] and natural pyrochlores,[17] as well as related structures,[18,19] indicate that pyrochlores with Ti, Nb, and Ta as the major B-site cations become amorphous as a result of the gradual accumulation of alpha-recoil collision cascades. However, such studies are time consuming, and only limited data under a few sets of experimental conditions are available. Heavy-ion irradiation studies,[6,13,20–24] which have been used to more rapidly evaluate radiation effects, have been completed on a wide range of pyrochlore compositions that generally confirm the results for the actinide-doped pyrochlores or natural minerals.

Considerable transmission electron microscope (TEM) studies have been carried out to characterize the temperature dependence of the critical dose for amorphization;[6,20–24] however, few studies have quantitatively investigated the damage evolution behavior as a function of irradiation dose at different temperatures, particularly in relevant pyrochlore phases. Quantitative characterization of damage accumulation as a function of dose and temperature, using ion-channeling methods in single crystals, should lead to a better understanding of the amorphization and damage evolution processes. Using single crystals of samarium titanate ($Sm_2Ti_2O_7$), the damage evolution on the Sm and O sublattices is characterized in the present study. In general, alpha decay of the actinide elements produces alpha particles with energies of 4.5 to 5.8 MeV and recoil nuclei (alpha recoils) with energies of 70 to 100 keV, and the more massive but lower energy alpha recoil accounts for most of the damage produced through elastic scattering collisions. Because the nuclear stopping of 1.0 MeV Au at the damage peak in $Sm_2Ti_2O_7$ is similar to the nuclear stopping of alpha recoils, the damage evolution on the Sm and O sublattices under 1.0 MeV Au irradiation is characterized at the damage peak region, which provides a reasonable simulation of the damage evolution behavior due to alpha recoils. The Au irradiations were carried out at 170, 300, and 700 K, and a disorder accumulation model was employed to characterize the defect accumulation and amorphization behavior.

II. EXPERIMENTAL PROCEDURES

The $Sm_2Ti_2O_7$ single crystals were grown by a floating zone technique using an infrared image furnace at the University of Warwick, UK. The growth was conducted in air at growth speeds of around 6–8 mm/h.[25] The pyrochlore crystal was sectioned along the (100) plane and the polished samples were characterized by high-resolution x-ray diffrac-

[a]Author to whom correspondence should be addressed; electronic mail: Yanwen.Zhang@pnl.gov

tion (HRXRD) and a series of pole figure measurements. Samples exhibiting large single crystal regions were then selected for the irradiation experiments. Powder XRD results revealed no evidence for the existence of secondary or minor phases, thereby confirming the single-phase nature of the crystals with a lattice parameter of 1.0233 nm.

The Au irradiations and subsequent investigation of damage accumulation in the $Sm_2Ti_2O_7$ single crystals were carried out using the 3.0 MV tandem accelerator facility within the Environmental Molecular Sciences Laboratory (EMSL) at the Pacific Northwest National Laboratory (PNNL). Each sample was mechanically mounted to a molybdenum plate using molybdenum spring-loaded clips, with a chromel-alumel thermocouple clamped to the sample surface. The samples were implanted at 170, 300, and 700 K with 1.0 MeV Au^{2+} ions at near normal incident angle to fluences ranging from 1×10^{12} to 8×10^{13} Au^{+} cm^{-2}, which produced damage states that ranged from relatively minor disorder to a fully amorphous buried layer. For each ion fluence, the local dose at the damage peak, in displacements per atom (dpa), was determined using the Stopping and Range of Ions in Matter (SRIM) 2003 code[26] under full-cascade mode, assuming a theoretical density of 6.305 g/cm^3 and threshold displacement energies of 50 eV for Sm, Ti, and O atoms.[10] The conversion factor at the damage peak from ion fluence (10^{14} Au^{+} cm^{-2}) to dose (dpa) is 0.45 under the irradiation conditions of this study. A low constant ion flux of 3×10^{11} $Au\,cm^{-2}\,s^{-1}$ was employed during each implantation to avoid beam heating. The beam energy was chosen to produce shallow damage that could be readily measured by ion-beam analysis methods.

The damage evolution was investigated from the relative disorder that was determined using Rutherford backscattering spectroscopy (RBS) and nuclear reaction analysis (NRA) along the ⟨001⟩ channel direction. The RBS interaction yield for heavy elements along a low-index crystallographic direction is sensitive to very small displacements of the atoms from crystalline lattice sites, which makes the technique unique for analysis of ion-implantation damage in single crystals. As a complement to RBS, NRA in a channeling geometry can be utilized to profile atomic disorder of light isotopes in matrices of compound substrates with heavy elements. The relative disorder measured by ion channeling methods is the appropriately corrected ratio of the aligned backscattering/reaction yield along a channeling direction to the random yield,[27–29] which is described in more detail below. For ion-beam induced damage, the backscattering/reaction yield is primarily due to interstitials within channels, unaligned atoms in amorphous domains, and unaligned atoms due to local strain from dislocations or bubbles. The ion-channeling methods are not as sensitive to vacancies, antisite defects, or the cation and anion disorder studied by others,[24] which are defect states on crystallographic sites; however, the influence of such defects can be noted in the dechanneling fraction or in the width of the channel. The disordering measured in the present study by ion channeling is disorder associated with anions and cations on noncrystalline sites.

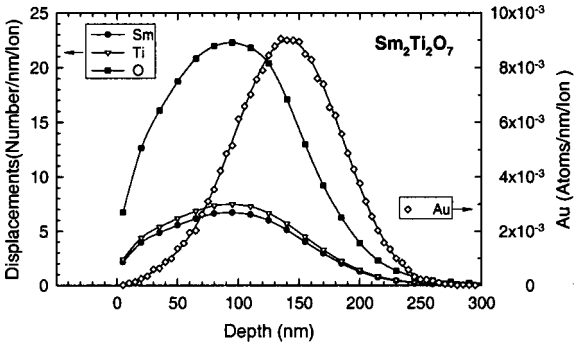

FIG. 1. Predicted recoil profiles of Sm, Ti, and O (left Y axis) from SRIM 2003 calculations for 1.0 MeV Au^{+} irradiated at a normal incident under full-cascade mode with a density of 6.305 g/cm^3 and threshold displacement energies of 50 eV for all Sm, Ti, and O sublattices, respectively. Also included is the Au distribution (right Y axis).

In the current study, RBS and the $^{16}O(d,P)^{17}O$ NRA were employed to investigate damage accumulation on the Sm and O sublattices along the ⟨001⟩ direction using 2.0 MeV He^{+} and 900 keV D^{+} with a scattering angle of 150°, respectively. The measurements were performed *in situ* under high vacuum in the target chamber. For the 170 and 300 K irradiated samples, the measurements were conducted at the same temperature as the irradiation temperature, while analysis for the 700 K irradiations was performed at room temperature. This procedure ensured that thermal recovery processes were quenched prior to analysis. Backscattering yields from the same virgin spot were used to check the damage sensitivity and stability of the crystal under exposure to the analyzing beam. Noticeable increases of the backscattering yield were observed when the dose from ion-beam analysis exceeded 5×10^{16} ion cm^{-2}, which is about six times more than the dose needed to collect a typical RBS/NRA spectrum.

Thermal recovery and ^{18}O exchange were studied using a sample irradiated with 800 keV Au^{+} ions at a normal incident angle to ion fluences of 1.5×10^{13} $Au\,cm^{-2}$. Isochronal annealing was carried out in an ^{18}O environment at a pressure of 4×10^{-6} Torr up to 970 K for 30 min. To investigate the exchange of ^{16}O in the sample with ^{18}O in the annealing environment, nuclear reaction analysis (NRA) $^{18}O(p,\alpha)^{15}N$ with a 745 keV H^{+} beam was employed. Thermal recovery on Sm sublattice was studied by RBS using a 2.0 MeV He^{+} beam along the ⟨001⟩ channeling geometry.

III. RESULTS AND DISCUSSION

A. Damage accumulation

The predicted profiles of damage and Au concentration in the $Sm_2Ti_2O_7$ under 1.0 MeV Au irradiation at a normal incident angle are shown in Fig. 1. The predicted profiles are based on full-cascade simulations using the SRIM 2003 code.[26] As shown in Fig. 1, the relative damage profiles of target recoils Sm, Ti, and O are peaked at ~95 nm, which have a shallower distribution than the predicted Au profile, which is peaked at ~140 nm. According to the calculations, 1.0 MeV Au^{+} implantation produces significant damage over its path, with over 5300 displacements per Au ion. Sig-

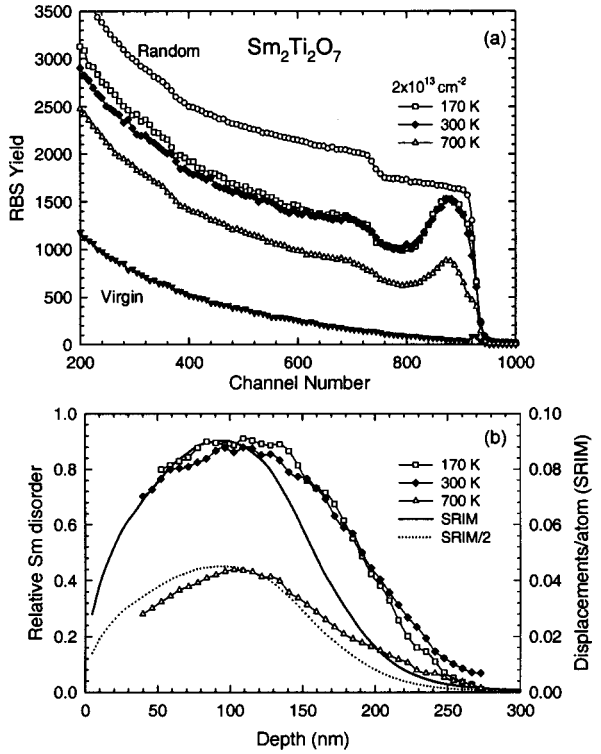

FIG. 2. (a) RBS spectra for samples irradiated with 1.0 MeV Au^+ to ion fluences of 2.00×10^{13} at 170, 300, and 700 K, respectively. The samples are analyzed using 2.0 MeV He^+ in ⟨001⟩ direction. Random and channeling spectra from a virgin area are also included. (b) The corresponding profiles of relative Sm disorder at 170, 300, and 700 K (left Y axis) and the SRIM predicted damage profile (right Y axis) for 1.0 MeV Au implantation to an ion fluence of 2.0×10^{13} (solid line), as well as a SRIM/2 profile (dotted line).

nificantly more O displacements, as compared with Sm and Ti displacements, are predicted by the simulations, which is primarily attributed to the higher abundance of oxygen.

The RBS spectra for samples implanted to an ion fluence of 2×10^{13} cm^{-2} at different temperatures are shown in Fig. 2(a), which illustrates the general statistics for other measurements. A random spectrum and a channeling spectrum taken from a virgin area are also included. The ratio of the backscattering yield in the virgin spectrum to the yield in the random spectrum just below the surface peak $\chi_{\min}$ is 0.037, which indicates the high quality of the virgin crystal. The emergence of the damage peaks in the channeling spectra indicates the presence of disorder that causes direct backscattering of the channeled ions. For the same ion fluence, there is a significant reduction of the backscattering yield at 700 K, as compared with 170 and 300 K, which indicates a much higher rate of dynamic recovery at 700 K. Because the damage accumulation at the surface increases with ion fluence, the surface peak cannot be resolved after irradiation to 2×10^{13} Au^+ cm^{-2}.

In order to obtain a quantitative damage profile, it is essential to determine the dechanneling component of the RBS spectra as a function of depth. Because the backscattering yield due to the ion-implantation-induced disordering is much more evident from the Sm sublattice, all analyses of cation disordering were performed on that part of the spectrum. The depth profiles of relative Sm disorder and the corresponding disorder at the damage peak were determined from the RBS spectra using an iterative procedure,[27–29] which provides a more reliable determination than the linear dechanneling approximation often employed. The iterative procedure starts from the surface channel and successively moves forward in depth to determine the dechanneling fraction in the next channel, which enables the direct backscattering contribution from the displaced atoms to be determined at that depth.[28,29] The continuous amorphous state is defined as achieving a relative disorder of 1.0, where the aligned spectrum overlaps with the random spectrum.

The relative Sm disorder profiles, derived from the RBS spectra in Fig. 2(a), are given in Fig. 2(b). The apparent depth scale is determined from the energy differences associated with the channel numbers, the He stopping powers in $Sm_2Ti_2O_7$ from SRIM, and assuming a sample density of 6.305 g cm^{-3}. The stopping powers of He in the aligned directions are assumed to be the same as in the random direction due to the uncertainty in establishing the differences for the various damage states. As shown in Fig. 2(b), the depth profile of the implantation-induced disorder has a maximum at about 105 nm. Comparing the profiles for the samples irradiated at different temperatures, a slight decrease in disorder at the damage peak is observed with increasing irradiation temperature from 170 to 300 K, and a significant decrease in relative disorder within the whole irradiated region is evident at 700 K. Damage accumulation is a direct result from the competition between the damage production and dynamic annealing processes during irradiation. Because the defect annihilation process is primarily thermally activated and there is a lack of thermal energy at and below room temperature for significant dynamic defect annealing, the lower defect annihilation rate leads to a much higher relative Sm disordering rate at 170 and 300 K. During irradiation at 700 K, dynamic recovery of point defects occurs at a much higher rate, which suppresses the rate of disordering during irradiation and leads to a significant decrease in accumulated disorder over the whole implanted region at 700 K, as shown qualitatively in Fig. 2(a) for the surface region (around channel 950) and quantitatively in Fig. 2(b) for the deeper implanted region.

Also shown in Fig. 2(b) is the SRIM predicted profile of displacements in $Sm_2Ti_2O_7$ implanted with Au ions to a fluence of 2×10^{13} cm^{-2} at a normal incident angle, which is approximately the sum of the recoil distributions of the target atoms Sm, Ti and O, as shown in Fig. 1. Comparing the profiles in Fig. 2(b), the experimental disorder profiles at 170 and 300 K have a deeper and boarder distribution (peak width of ~180 nm) than the SRIM predictions (peak width of ~148 nm), which might be due to significant error in the SRIM stopping powers for He and/or Au in $Sm_2Ti_2O_7$. It is worth noting that different Y-axis scales are used in Fig. 2(b) for the experimental data and the SRIM results. This indicates that the average damage production rate is much higher under the 170 and 300 K Au irradiation than the SRIM prediction, which is based solely on the production of displaced atoms in a perfect crystal. The differences in damage production rates between the measurements and simulations are pri-

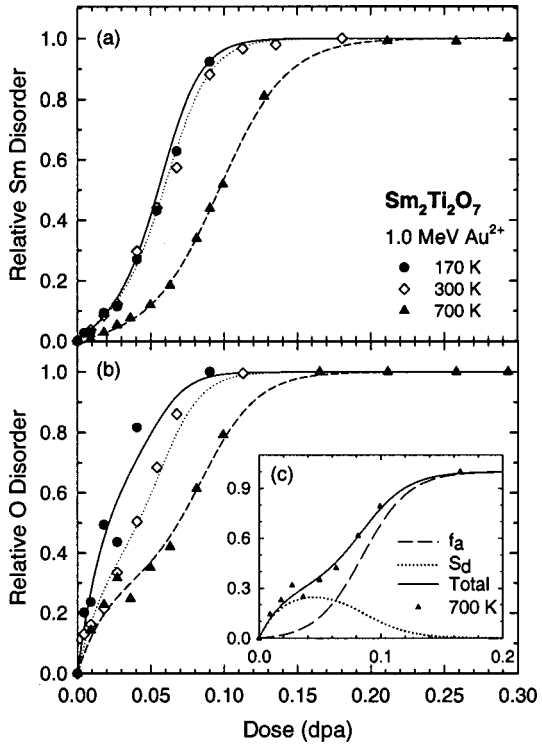

FIG. 3. Relative disorder at the damage peak on (a) Sm and (b) O sublattices as a function of local dose for $Sm_2Ti_2O_7$ single crystals implanted with 1.0 MeV Au^+ at 170, 300, and 700 K. Solid lines are fits of Eq. (1) to the data, using Eqs. (2) and (3). The O data at 700 K is shown in (c) with the fits of the total disorder (S), the amorphous fraction (f_a), and the relative disorder from irradiation-induced interstitials and clusters (S_d).

marily attributed to the contribution of defect-stimulated amorphization to the relative disorder at different irradiation temperatures. The SRIM profile divided by two (equivalent to a fluence of 1×10^{13} cm^{-2}) is also plotted for convenient comparison to the shape of the 700 K profile. In the near surface region (a few tens of nanometers), the damage accumulation at 700 K is suppressed, which may suggest increased defect annihilation at the surface. The narrower disorder profile for irradiation at 700 K (peak width of ~145 nm), as compared with the lower temperature irradiations (peak width of ~180 nm), is likely due to a combination of the nonlinear accumulation of relative disorder and significant dynamic annealing, which results in different damage production to recovery ratios at different depths that lead to decreased local damage accumulation rate away from the damage peak. The deeper damage peak for the 700 K spectrum than the SRIM prediction may be attributed to discrepancies in the electronic stopping powers, as discussed above.

B. Modeling behavior at the damage peak

The relative disorder S in the $Sm_2Ti_2O_7$ crystals on the Sm and O sublattices at the damage peak is shown in Fig. 3 as a function of local dose. The relative O disorder at the damage peak was determined from the NRA spectra using the ratio of aligned spectra to random spectra and correcting for the background-dechanneling fraction. The results in Fig. 3 indicate that the atomic disorder on both the Sm and O sublattices increases nonlinearly with dose, eventually achieving a fully amorphous state. The solid lines in Fig. 3 are the fits to a disorder accumulation model. The total relative disorder S produced under ion-beam irradiation and measured by ion-channeling methods consists of contributions from irradiation-amorphized and damaged-crystalline regions according to the following expression:

$$S = f_a + S_d + S_c, \tag{1}$$

where f_a is the amorphous fraction, and S_d is the relative disorder from irradiation-induced interstitials and the small interstitial clusters in the residual crystalline regions. The third term S_c accounts for the relative disorder from the growth of extended defect clusters, which may be a significant contribution at irradiation temperatures close to the critical temperature for amorphization, where point defects are more mobile. Under the current study, the contribution of S_c to the total disorder is insignificant and will not be discussed further.

The amorphous fraction can be described using a direct-impact, defect-stimulated (DI/DS) model for amorphization.[30] In this model, amorphous nuclei are directly produced in the core of a cascade, and the irradiation-induced point defects accumulate and stimulate further amorphization at the crystalline-amorphous interfaces. The amorphous fraction is given by the following expression:[30]

$$f_a = 1 - (\sigma_a + \sigma_s)/\{\sigma_s + \sigma_a \exp[(\sigma_a + \sigma_s)D]\}, \tag{2}$$

where σ_a is the amorphization cross section, σ_s is the effective cross section for defect-stimulated amorphization, and D is the local dose (dpa).

The relative disorder S_d is primarily due to the accumulation of interstitial defects. Irradiation leads to the formation and accumulation of Frenkel pairs in the residual crystalline material. Spontaneous recombination of interstitials and vacancies within a recombination volume leads to a steady state defect concentration that is temperature dependent. This process can be described using a simple defect accumulation model[31,32] that is consistent with the observed behavior for the accumulation of point defects in $Gd_2Ti_2O_7$[33] and other related materials.[19,32] The relative disorder contribution S_d is given by this simple defect accumulation model multiplied by the probability $(1-f_a)$ for a defect being produced in the residual crystalline material[34]

$$S_d = S_d^*[1 - \exp(-BD)](1 - f_a), \tag{3}$$

where S_d^* is the saturation value for the defect-induced disorder observed along a specified channel direction, which is proportional to the local displacement rate, and B (dpa^{-1}) is proportional to an effective recombination volume for the specific defects giving rise to S_d.

The curves shown in Fig. 3 are fits of the above model to the data, and the model parameters are summarized in Table I. There is considerable uncertainty in these fit parameters at this time due to the limited data for the pyrochlore system, but it is expected that the uncertainty will be reduced as more experimental data are obtained and analyzed. The significantly larger values for σ_s relative to σ_a in Table I indicate the significant contribution of defect-stimulated processes to amorphization in $Sm_2Ti_2O_7$ pyrochlore. Previous *in situ*

TABLE I. Model parameters from fits of Eq. (1) to data in Fig. 3.

Sm Sublattice	170 K	300 K	700 K
σ_a (dpa^{-1})	1.0	1.0	0.6
σ_s (dpa^{-1})	72.0	66.0	43.2
S_d^*	0.30	0.28	0.061
B (dpa^{-1})	10	10	10
O Sublattice			
σ_a (dpa^{-1})	1.0	1.0	0.6
σ_s (dpa^{-1})	79.0	72.0	51.8
S_d^*	0.72	0.42	0.30
B (dpa^{-1})	50	50	50

TEM studies of amorphization in $Sm_2Ti_2O_7$ under Bi^+ and Kr^+ irradiation[10,35] indicate that this material exhibits isolated damage clusters with sizes of a few nanometers in diameter at low doses. Growth of the clusters results in the appearance of diffuse rings in the electron diffraction patterns with increasing dose. In parallel with the amorphization process, the crystalline structure undergoes an irradiation-induced order-disorder structural transformation to the defect-fluorite structure due to defect accumulation in the residual crystalline material. The structural transformation is due to the disordering of Sm and Ti on cation sites and O on the occupied and vacant anion sites,[36,37] where the relaxation of cation interstitials onto vacant sites of the opposite cation leads to cation disordering and the relaxation of oxygen interstitials onto the vacant $8a$ sites leads to anion disorder. This behavior is consistent with a small cross section for direct-impact amorphization (σ_a), which describes the volume of the amorphous cascade core, and the relatively large cross section for defect-stimulated processes (σ_s), which contributes to both the structural transformation and the growth of amorphization domains. The value for σ_a suggests an amorphous core of about 2 nm in diameter, which is consistent with the observed size of direct-impact amorphous cores in ion-irradiated natural pyrochlores.[38] It is also evident in Table I that the value of S_d^* for the O sublattice is larger than for the Sm sublattice. Because the amorphous state should be stoichiometric, amorphization cannot account for the higher O disorder. There are three possible explanations for the higher relative disorder measured by ion-channeling methods: (1) the displacement energies may be much lower on the O sublattice relative to Sm (or Ti); (2) the configuration of the O interstitial defects is such that they are more readily observed along this channeling direction than the cation interstitial defects; or (3) the O interstitial defects are more stable (less close-pair recombination) than the cation interstitial defects. While theoretical results[36] predict a lower minimum displacement energy for oxygen, a recent experimental study[39] at room temperature suggests a threshold displacement energy of 47 ± 5 eV for O in pyrochlores, which is consistent with the value assumed in the present study; thus, the displacement energy for Sm (and Ti) may be larger than assumed, but more theoretical work would be required to validate this. Significant anion disordering on the oxygen sublattice was reported as a result of ion irradiation;[24] however, such disordering would not contribute to the measured backscattering yield. The high density of oxygen atoms in the structure may lead to more highly separated (and thus stable) oxygen Frenkel pairs from collision sequences. This could also account for a higher survivability of oxygen interstitials, which is supported somewhat by recent computer simulations of cascades in a pyrochlore.[36] Determining the stable configurations of cation and anion interstitial defects will be necessary to ascertain if the stable anion configurations are more readily measured along [001] relative to the cation interstitials. Such work will require exhaustive theoretical calculations that are beyond the scope of the present article. The higher B values for the O sublattice than the Sm sublattice indicate a larger effective recombination volume for O interstitials under the current irradiation conditions, which suggests lower barriers for recombination. Based on the model fits, the decrease in amorphization rate at 700 K is associated with decreases in the values of σ_a, σ_s, and S_d^* for both the Sm and O sublattices.

One of the striking observations in the irradiations at all three temperatures is the deviation in the dose dependence of the O disorder at low doses from the simple sigmoidal dependence, as shown in Fig. 3(b). Based on the model, this behavior is attributed to a significant accumulation of irradiation-induced O interstitials. Using the 700 K data as an example, the contributions to the total disorder from amorphous (f_a) and crystalline regions (S_d) are shown in Fig. 3(c). It is evident that at low doses, the relative disorder from irradiation-induced interstitials and interstitial clusters play an important role. As the irradiation dose increases, the crystalline fraction ($1-f_a$) decreases due to the increasing amorphous fraction, and the contribution from the interstitials defects (S_d) decreases. As shown in Fig. 3(c), the amorphous contribution (f_a) to disorder becomes dominant at doses higher than ~0.1 dpa at this temperature.

C. Critical dose and temperature

The temperature dependence of achieving a relative disorder level of 0.99, just below the critical dose for amorphization, is shown in Fig. 4(a). As RBS with He^+ ions provides more reliable data than the NRA results, the relative disorder level and the corresponding dose are based on the Sm data and the corresponding fits in Fig. 3(a). The value of 0.99 was chosen to define the critical amorphization dose because the exponential dependence of the disorder on dose increases the error in defining a dose for complete amorphization, as the disorder approaches 1.0. As shown in Fig. 3(a), the critical dose for amorphization is 0.14 dpa for 170 and 300 K irradiation and 0.22 dpa for 700 K irradiation. These critical dose values are plotted in Fig. 4, along with previous *in situ* TEM results for $Sm_2Ti_2O_7$ irradiated with 0.6 MeV Bi^+ ions[10] and the amorphization dose due to alpha decay in $Gd_2Ti_2O_7$ doped with 3 wt % ^{244}Cm.[33] Considering the uncertainties in the dose measurements and the differences in defining amorphization by RBS and TEM techniques, the results indicate reasonable agreement between the two techniques. In general, the results in Fig. 4 show that amorphization under the heavy-ion irradiation conditions is relatively independent of the dose rate at temperatures sig-

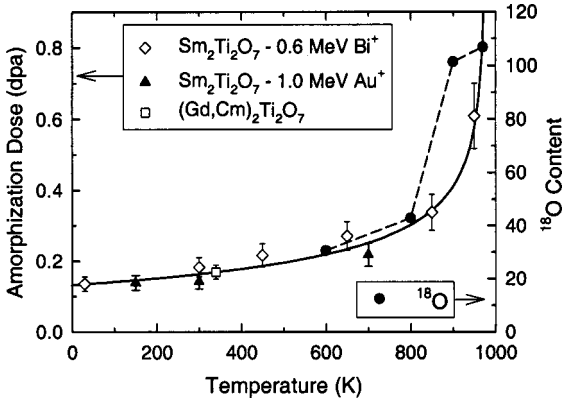

FIG. 4. Temperature dependence of the dose to achieve a relative disorder level of 0.99 in $Sm_2Ti_2O_7$ under 1.0 MeV Au^+ irradiation, along with previous results for amorphization dose under 0.6 MeV Bi^+ irradiation[10] and the dose for amorphization in $Gd_2Ti_2O_7$ doped with 3 wt % ^{244}Cm.[33] Also included is the ^{18}O uptake, the total NRA yield in the implanted region, during isochronal annealing.

nificantly below the critical temperature for amorphization (T_c), which is defined where the amorphization rate equals the damage recovery rate. For $Sm_2Ti_2O_7$ pyrochlore, the value of T_c under Bi^+ irradiation[10] has been previously determined to be ~950 K, as illustrated in Fig. 4.

One of the main reasons for investigating defect accumulation and amorphization mechanisms under ion irradiation is to establish and examine theoretical models that predict the behavior of materials for the immobilization of actinides over long time periods. Since the experimental studies accelerate the damage rates by orders of magnitude compared with the alpha-decay rate of actinide waste forms, the usefulness of ion-beam results to predict behavior in actinide waste forms may be questioned. Irradiation studies indicate that the damage recovery processes affecting amorphization may be associated with both irradiation-assisted and thermal recovery processes.[30] If irradiation-assisted processes dominate, T_c is independent of the damage rate and, consequently, cannot be used to predict the critical temperature under lower dose-rate conditions, where irradiation-assisted processes are negligible. On the other hand, when thermal recovery processes dominate, T_c is strongly dependent on damage rate and largely independent of ion mass, as has been shown for $Gd_2Ti_2O_7$,[33] and the dose for amorphization is relatively independent of dose rate at temperatures below T_c. Despite the six orders of magnitude difference in damage rates, the good agreement between the amorphization doses near room temperature in $Sm_2Ti_2O_7$ under ion irradiation (0.6 MeV Bi^+ and 1.0 MeV Au^{2+}) and in $Gd_2Ti_2O_7$ due to ^{244}Cm decay, as shown in Fig. 4, confirms some degree of dose-rate independence below T_c, which provides some validation for using the results from ion irradiation studies in rare-earth titanates to predict long-term behavior due to alpha decay. Furthermore, heavy-ion irradiation studies have generally shown no significant effect of A-site ion mass on the temperature dependence of the critical dose for amorphization in rare-earth titanates.[10] Because of the similarity in behavior for $Sm_2Ti_2O_7$ and $Gd_2Ti_2O_7$,[10] and the lack of a significant ion mass effect in $Gd_2Ti_2O_7$,[33] the T_c for the Au^+ irradiation conditions in the present study is expected to be defined by that for Bi^+ ions (Fig. 4). The results from Fig. 4 suggest that irradiation-assisted recovery processes are insignificant and that thermal recovery processes play an important role in the damage evolution processes in $Sm_2Ti_2O_7$ pyrochlore. Thus, the shift in T_c for lower dose rates associated with alpha decay in actinide-containing rare-earth titanates can be evaluated using available models.[30]

D. Oxygen exchange

The temperature dependence of the exchange between ^{16}O in the sample and ^{18}O in the annealing environment was studied by isochronal annealing for 30 min. As shown in Fig. 4, there is a significantly increased ^{18}O exchange between 800 and 900 K due to an increase in the thermal mobility of oxygen vacancies. Because this increase in thermal mobility of O vacancies occurs just below the critical temperature, where higher defect mobilities (recovery rates) are required to balance the damage production rate, the ^{18}O uptake results suggest a strong correlation between T_c and the mobility of oxygen vacancies. This is also consistent with the observation of similar values of T_c for several $A_2Ti_2O_7$ pyrochlores (A=Y, Sm, Gd, and Lu),[10] which have similar activation energies for migration of oxygen vacancies.[37] While these results suggest a role of oxygen vacancy mobility in defining T_c, a role for the mobility of cation interstitials or vacancies has not been ruled out. Further studies, which are planned, on oxygen and cation vacancy mobilities will provide more definitive data on the processes that define T_c in these materials.

IV. CONCLUSIONS

Single crystals of $Sm_2Ti_2O_7$ were irradiated with 1.0 MeV Au^+ at 170, 300, and 700 K to study the accumulation of atomic disorder on both the Sm and O sublattices using *in situ* RBS and NRA along the ⟨001⟩. The results show that the atomic disorder on both the Sm and O sublattices increases nonlinearly with ion fluence, eventually achieving a fully amorphous state. The nonlinear damage evolution is consistent with a disorder accumulation model, which indicates a significant role of defect-stimulated amorphization processes. The quantitative details on the damage accumulation processes provide a better understanding of the defects and amorphization processes, which accumulation can be used to assess the impact of alpha-decay events on long-term performance. At low ion fluences, the disorder on the O sublattice is higher than that for Sm, which suggests differences in threshold displacement energies, defect configurations, or defect stability between the O and Sm sublattices. As compared with the 170 and 300 K irradiations, the rate of damage accumulation at 700 K decreases dramatically due to significant dynamic recovery. The critical dose for amorphization is ~0.14 dpa for 170 and 300 K irradiation and 0.22 dpa for 700 K irradiation, which are in good agreement with additional *in situ* TEM results for polycrystalline $Sm_2Ti_2O_7$ irradiated with 600 keV Bi^+ ions and for ^{244}Cm-containing $Gd_2Ti_2O_7$. The increase in exchange between ^{16}O in the

sample and ^{18}O near the critical temperature for amorphization suggests a correlation between oxygen vacancy mobility and the critical temperature.

ACKNOWLEDGMENTS

The authors would like to thank D. E. McCready for evaluating single crystal quality. This work was supported by the Division of Materials Sciences and Engineering, Office of Basic Energy Sciences, U.S. Department of Energy. Support for the accelerator facilities within the Environmental Molecular Sciences Laboratory (EMSL) was provided by the Office of Biological and Environmental Research. The Pacific Northwest National Laboratory is operated by Battelle Memorial Institute for the U.S. Department of Energy under Contract No. DE-AC 06-76RLO1830.

[1] H. L. Tuller, J. Phys. Chem. Solids **55**, 1393 (1994).
[2] B. J. Wuensch, K. W. Eberman, C. Heremans, E. M. Ku, P. Onnerud, E. M. E. Yeo, S. M. Haile, J. K. Stalick, and J. D. Jorgensen, Solid State Ionics **129**, 111 (2000).
[3] J. B. Goodenough and R. N. Castellano, Solid State Chem. **44**, 109 (1982).
[4] S. J. Korf, H. J. A. Koopmans, B. C. Lippens, A. J. Burggraaf, and P. J. Gellings, J. Chem. Soc., Faraday Trans. **83**, 1485 (1987).
[5] K. E. Sickafus, L. Minervini, R. W. Grimes, J. A. Valdez, M. Ishimaru, F. Li, K. J. McClellan, and T. Hartmann, Science **289**, 748 (2000).
[6] S. X. Wang, B. D. Begg, L. M. Wang, R. C. Ewing, W. J. Weber, and K. V. Govidan Kutty, J. Mater. Res. **14**, 4470 (1990).
[7] A. B. Harker, in *Radioactive Waste Forms for the Future*, edited by W. Lutze and R. C. Ewing (North-Holland, Amsterdam, 1988), p. 335.
[8] B. R. Myers, G. A. Armantrout, C. M. Jantzen, A. Jostsons, J. M. McKibben, H. F. Shaw, D. M. Strachan, and J. D. Vienna, Technical Evaluation Panel Summary Report, Plutonium Immobilization Project, Report No. UCRL-ID-129315, 1998.
[9] R. C. Ewing, W. J. Weber, W. Lutze, in *Diposal of Weapon Plutonium*, edited by E. R. Merz and C. E. Walter (Kluwer Academic, The Netherlands, 1996), p. 65.
[10] B. D. Begg, N. J. Hess, W. J. Weber, R. Devanathan, J. P. Icenhower, S. Thevuthasan, and B. P. McGrail, J. Nucl. Mater. **288**, 208 (2001).
[11] W. J. Weber, J. W. Wald, and Hj. Matzke, Mater. Lett. **3**, 173 (1985).
[12] W. J. Weber, J. W. Wald, and Hj. Matzke, J. Nucl. Mater. **138**, 196 (1986).
[13] B. D. Begg, W. J. Weber, R. Devanathan, J. P. Icenhower, S. Thevuthasan, and B. P. McGrail, Ceram. Trans. **107**, 553 (2000).
[14] R. C. Ewing, W. J. Weber, and F. W. Clinard, Jr., Prog. Nucl. Energy **29**, 63 (1995).
[15] W. J. Weber, R. C. Ewing, C. R. A. Catlow, T. Diaz de la Rubia, L. W. Hobbs, C. Kinoshita, Hj. Matzke, A. T. Motta, M. Nastasi, E. K. H. Salje, E. R. Vance, and S. J. Zinkle, J. Mater. Res. **13**, 1434 (1998).
[16] J. P. Icenhower, D. M. Strachan, M. M. Lindberg, E. A. Rodriguez, and J. L. Steele, *Dissolution Kinetics of Titanate-Based Ceramic Waste Forms: Results from Single-Pass Flow Tests on Radiation Damaged Specimens*, PNNL-14252 (Pacific Northwest National Laboratory, Richland, WA, 2003).
[17] G. R. Lumpkin, J. Nucl. Mater. **289**, 136 (2001).
[18] F. W. Clinard Jr., D. L. Rohr, and R. B. Roof, Nucl. Instrum. Methods Phys. Res. B **581**, 1 (1984).
[19] F. W. Clinard Jr., D. E. Peterson, D. L. Rohr, and L. W. Hobbs, J. Nucl. Mater. **126**, 245 (1984).
[20] R. C. Ewing and L. M. Wang, Nucl. Instrum. Methods Phys. Res. B **65**, 319 (1992).
[21] S. X. Wang, L. M. Wang, R. C. Ewing, G. S. Was, and G. R. Lumpkin, Nucl. Instrum. Methods Phys. Res. B **148**, 704 (1999).
[22] S. X. Wang, L. M. Wang, R. C. Ewing, and K. V. Govidan Kutty, Mater. Res. Soc. Symp. Proc. **540**, 355 (1999).
[23] W. J. Weber and N. J. Hess, Nucl. Instrum. Methods Phys. Res. B **80–81**, 1245 (1993).
[24] J. Lian, L. Wang, J. Chen, K. Sun, R. C. Ewing, J Matt Farmer, L. A. Boatner, Acta Mater. **51**, 1493 (2003).
[25] G. Balakrishnan, O. A. Petrenko, M. R. Lees, and D. M. Paul, J. Phys.: Condens. Matter **10**, L723–L725 (1998).
[26] J. F. Ziegler, J. P. Biersack, and U. Littmark, *The Stopping and Range of Ions in Solids* (Pergamon, New York, 1985).
[27] L. C. Feldman, J. W. Mayer, and S. T. Picraux, *Materials Analysis by Ion Channeling* (Academic Press, New York, 1982), p. 117.
[28] M. L. Swanson, in Handbook of Modern Ion Beam Materials Analysis, edited by J. R. Tesmer and M. Nastasi (Materials Research Society, Pittsburgh, PA, 1995), p. 263.
[29] J. S. Williams and R. G. Elliman, in *Ion Beams for Materials Analysis*, edited by J. R. Bird and J. S. Williams (Academic Press, Australia, 1989), p. 286.
[30] W. J. Weber, Nucl. Instrum. Methods Phys. Res. B **166–167**, 98 (2000).
[31] F. L. Vook and H. J. Stein, Radiat. Eff. **2**, 23 (1969).
[32] W. J. Weber, J. Nucl. Mater. **98**, 206 (1981).
[33] W. J. Weber and R. C. Ewing, Mater. Res. Soc. Symp. Proc. **713 2002, p.** 443.
[34] Y. Zhang, W. J. Weber, W. Jiang, A. Hallén, and G. Possnert, J. Appl. Phys. **91**, 6388 (2002).
[35] S. X. Wang, L. M. Wang, R. C. Ewing, and K. V. Govidan Kutty, Nucl. Instrum. Methods Phys. Res. B **169**, 135 (2000).
[36] A. Chartier, C. Meis, J.-P. Crocombette, L. R. Corrales, and W. J. Weber, Phys. Rev. B **67**, 174 102 (2003).
[37] M. Pirzada, R. W. Grimes, L. Minervini, J. F. Maguire, and K. E. Sickafus, Solid State Ionics **140**, 201 (2001).
[38] S. X. Wang, L. M. Wang, and R. C. Ewing, J. Non-Cryst. Solids **274**, 238 (2000).
[39] K. L. Smith, M. Colella, R. Cooper, and E. R. Vance, J. Nucl. Mater. **321**, 19 (2003).